Molecular Therapy
Oncology
Original Article

Class I HDAC inhibition enhances the stem-like memory properties of CRISPR-engineered CAR T cells in neuroblastoma

Dan Cappabianca,[1,2] Mahmoud Toulany,[1,2] Seth Zima,[2,3,4] Amanda Shea,[1,2] Jolanta Vidugiriene,[5] Anthony Lauer,[5] Kayla Sylvester,[5] Varun Gnanasekar,[1,2] Sean Foster,[1,2] Rithvik Turaga,[2,3,4] Krishanu Saha,[2,3,6] Jose Ayuso,[2,3,4] and Quaovi H. Sodji[1,2]

[1]Department of Human Oncology, University of Wisconsin-Madison, Madison, WI 53705, USA; [2]Carbone Cancer Center, University of Wisconsin-Madison, Madison, WI 53705, USA; [3]Department of Biomedical Engineering, University of Wisconsin-Madison, Madison, WI 53715, USA; [4]Department of Dermatology, University of Wisconsin-Madison, Madison, WI 53705, USA; [5]Promega Corporation, Fitchburg, WI 53711, USA; [6]Wisconsin Institute for Discovery, University of Wisconsin-Madison, Madison, WI 53715, USA

Manufacturing chimeric antigen receptor (CAR) T cells with a stem cell memory phenotype can enhance their persistence in patients. Histone deacetylase inhibitors (HDACis) targeting class I HDACs promote chromatin remodeling in virally manufactured CAR T cells, leading to the activation of the Wnt pathway, and ultimately improve CAR T cell persistence. However, it is unknown whether the persistence of CRISPR-engineered CAR T cells can also be enhanced through such HDACi-mediated epigenetic modulation. CAR T cells engineered using CRISPR-Cas9 to integrate a CAR construct into the T cell receptor alpha constant (*TRAC*) were treated with various class- or isoform-selective HDACis, and phenotypic, functional, and metabolic changes were assessed *in vitro* and in a GD2+ neuroblastoma xenograft model. Compared to untreated GD2 *TRAC*-CAR T cells, chidamide and mocetinostat increased the stem cell memory marker expression ($CD62L^+$/$CCR7^+$/IL-$7R\alpha^+$). Chidamide induced a fragmented mitochondrial morphology and, *in vivo*, enhanced the persistence and naive phenotype of the GD2 *TRAC*-CAR T cells without upregulating exhaustion markers (PD-1/LAG3). These findings suggest that in the management of treatment-resistant pediatric solid tumors, utilizing chidamide during the manufacturing of CRISPR-engineered CAR T cells may enhance their persistence while retaining a naive phenotype.

INTRODUCTION

Chimeric antigen receptor (CAR) T cell therapy has revolutionized cancer treatment in the last decade and has become an essential pillar for hematological malignancies, including lymphoma and multiple myeloma.[1] Despite their success in hematological cancers, CAR T cells have not been as effective against solid tumors partly due to poor persistence and exhaustion in the immunosuppressive tumor microenvironment (TME).[2,3] Neuroblastoma (NB), the most common extracranial pediatric solid tumor, universally overexpresses the disialoganglioside GD2, which has been targeted by CAR T cells in pre-clinical studies.[4,5] Clinically, high-risk and relapsed NB is associated with a poor prognosis characterized by a 5-year survival around 50%.[6,7] Although clinical trials have evaluated the safety and efficacy of CAR T cells targeting GD2, outcomes remain poor.[4,8] Recently, Locatelli et al. reported the results of a phase 1/2 trial of a third-generation, virally manufactured GD2-targeting CAR T cell in high-risk metastatic, relapsed, or refractory NB in children. The overall response rate was 66%, and after a median follow-up of 4.2 years, the 5-year overall survival rate was 42.7%.[9] The GD2 CAR T cells persisted longer than a year in most patients, and in some cases 5 years post-CAR T cell infusion.[9] Such remarkable persistence has been previously attributed to the relative level of stem cell memory phenotype of the CAR T cells (T_{SCM}) generated during *ex vivo* manufacturing.[10–12]

A higher percentage of T_{SCM} in the pre-infusion product correlates with better long-term persistence in patients and can be characterized by the simultaneous expression of surface markers such as CD62L, CCR7, and IL-7Rα ($CD62L^+$/$CCR7^+$/IL-$7R\alpha^+$).[12] *Ex vivo* manufacturing of CAR T cells can be tailored to enrich for a T_{SCM} phenotype and metabolically fit phenotype by supplementing different cytokines,[12] inhibiting glycolytic pathways, brief metabolite deprivations,[13–16] or treatment with various small molecules.[17–19] Among these small molecules are histone deacetylase inhibitors (HDACis), especially class I isoform inhibitors, which increase the stem cell memory phenotype of virally manufactured CD19 and GD2 CAR T cells by activating the Wnt/β-catenin pathway.[20] The selective targeting of class I HDAC increased the retention of stem cell memory phenotype *ex vivo*, differentiation toward central memory status *in vivo*, potency *in vitro* and *in vivo*, resistance to exhaustion, and persistence of CAR T cells *in vivo*.[20] HDACs are epigenetic

Received 30 September 2025; accepted 2 April 2026;
https://doi.org/10.1016/j.omton.2026.201200.

Correspondence: Quaovi H. Sodji, Department of Human Oncology, University of Wisconsin-Madison, Madison, WI 53705, USA.
E-mail: qsodji@humonc.wisc.edu

regulators involved in various cellular processes including cell differentiation, metabolic homeostasis, cancer progression, neurodegeneration, immunological function, and other biological functions. They remove acetyl moieties from lysine residues on histones, resulting in a condensed and tightly packed chromatin structure that leads to transcriptional repression and gene silencing.[21] Based on their cofactor dependency, HDACs can be dichotomized into two groups, NAD^+-dependent (class III) and zinc-dependent, which can be further divided into class I, II, and IV based on their sequence homologies and cellular localization.[21,22]

All Food and Drug Administration (FDA)-approved gene vectors for CAR manufacturing are γ-retroviral or lentiviral-based, which insert into random loci in the genome and can cause insertional oncogenesis and heterogeneous CAR expression.[23,24] An alternate strategy uses CRISPR/Cas9 to insert gene vectors at the T cell receptor α constant (*TRAC*) locus via homology-directed DNA repair mechanism more reliably than viral vectors.[25–27] By knocking out the T cell receptor (TCR), this approach limits excessive tonic signaling seen in GD2 CAR T cells that can lead to anergy and exhaustion *in vivo*.[28] Additionally, transcription is controlled by the endogenous *TRAC* promoter, resulting in lower signaling than a constitutive promoter without affecting potency.[29] The efficacy of this approach was recently demonstrated in a $GD2^+$ NB xenograft model, where the subsequently generated CAR T cells (GD2 *TRAC*-CAR T cells) were less exhausted and had a greater percentage of T_{SCM} compared to virally manufactured GD2 CAR T cells.[26]

The aforementioned increase in the stem cell memory phenotype with HDACis has only been observed in virally manufactured CAR T cells, so it is unknown whether these findings could be generalized toward virus-free CRISPR CAR T cells. Given the stem-like state of CRISPR-engineered *TRAC*-CAR T cells and reduction in differentiation/exhaustion *in vivo* due to TCR knockdown,[26,29] an HDACi-induced phenotype may be more sustained in *TRAC*-CAR T cells than in virus-derived CAR T cells. Additionally, the lack of an endogenous TCR in *TRAC*-CAR T cells also affects NAD(P)H binding and cytoplasm size,[30] suggesting that HDACi may modulate *TRAC*-CAR T cell phenotypes differently. Herein, we manufactured virus-free CRISPR CAR T cells where the CAR construct (GD2 CAR) was inserted into the *TRAC* locus and evaluated whether the inhibition of selected classes of zinc-dependent HDAC would further enhance the stem-like properties of CRISPR-based GD2-CAR T cells. We found that the class I (HDAC1/2/3) and HDAC10 inhibitor, chidamide, enhanced the stem cell memory phenotype *in vitro* while enhancing persistence and the proportion of less differentiated cells *in vivo*. These findings hold promise for enhancing the longevity and efficacy of *TRAC*-CAR T cell therapies for solid tumors.

RESULTS

Class I HDAC inhibitors enhance stem-like phenotypes

A desirable CAR T cell pre-infusion product should have a balance of potent memory/effector cells, with stem-like phenotype, for optimal therapeutic efficacy.[10,12] We manufactured GD2 *TRAC* CAR T cells by electroporating primary T cells isolated from healthy donors in the presence of a CRISPR/Cas9 ribonucleoprotein (RNP) targeted to the *TRAC* locus and a homology-directed repair template encoding a GD2 CAR as previously done (Figure S1).[14] GD2 *TRAC* CAR T cells manufactured from different donors were cryopreserved on day 14 for subsequent use. Upon thawing, the GD2 *TRAC*-CAR T cells were allowed to rest for 24 h before a 3-day treatment with HDACis (Figure 1A). Five small molecule inhibitors targeting different HDAC isoforms were used, including (1) chidamide, HDAC 1/2/3 (class I) and HDAC10 (class IIb); (2) mocetinostat HDAC 1/2/3 (class I), and HDAC 11 (class IV); (3) PCI-34051, HDAC 8 (class I); (4) tubastatin A, HDAC 6 (class IIb); and (5) vorinostat, pan-isoform inhibitor. The GD2 *TRAC*-CAR T cells were treated with eight different concentrations (ranging from 10^{-2} to 10^5 nM) of each inhibitor, and their viabilities were assessed after 72 h using a CCK8 assay to generate IC_{50} curves (Figure S2). A sub-therapeutic concentration of each inhibitor was selected to minimize cell death while preserving biological effects and subsequently used throughout the conducted studies (Table S1). We observed that the treatment of GD2 *TRAC*-CAR T cells with the aforementioned sub-therapeutic dose of each inhibitor was not detrimental to the GD2 *TRAC*-CAR T cell viability (chidamide: 2.0-fold [0.5], mocetinostat: 1.7-fold [0.3], PCI-34051: 2.0-fold [0.3], tubastatin A: 1.7-fold [0.4], vorinostat: 1.7-fold [0.7], and untreated: 1.8-fold [0.1]) or expansion (chidamide: 64.7% [3.1], mocetinostat: 64.3% [8.5], PCI-34051: 69.0% [2.6], tubastatin A: 62.0%[3.0], vorinostat: 65.3% [4.9], and untreated: 61.0% [6.1]) (Figure S3).

The differentially treated GD2 *TRAC*-CAR T cells were stained to evaluate the expression of various markers of memory, exhaustion, activation, and cytotoxicity, including CD45RO, CD45RA, LAG3, PD-1, KLRG1, CD62L, CCR7, IL-7Rα, NKG2D, TRAIL, FASL, and HLA-DR, and subsequently analyzed by spectral flow cytometry. The expression of these markers was determined by the analysis of GD2 *TRAC*-CAR T cells that were gated as live cells, lacking the TCR (TCR^-) and expressing the CAR (CAR+) (Figure S4). In a reduced two-dimensional t-distributed stochastic neighbor embedding (t-SNE) space, single cells were separated based on apparent differences in surface marker expression and analyzed to assess whether differential HDACi treatment led to any global differences in the expression of the T_{SCM} markers. While GD2 *TRAC*-CAR T cells from each treatment overlapped and spanned most of the t-SNE space, PCI-34051-treated cells did not occupy the lower right corner (Figure 1B). Interestingly, chidamide and mocetinostat, relative to other treatments, had a higher number of cells in the lower right corner (Figure 1B). Notably, this area represented about 93% of cells with co-expression of three markers for T_{SCM}: CD62L, CCR7, and IL-7Rα (Figures 1C and S5). Consequently, we quantified the percentage change in T_{SCM} markers and observed that both chidamide and mocetinostat increased the co-expression of T_{SCM} markers by over 80% relative to untreated GD2 *TRAC*-CAR T cells, which was a significantly higher increase compared to PCI-34051 and tubastatin A: T_{SCM}: (chidamide: 81.2% [28.9], mocetinostat: 80.1% [38.8], PCI-34051: −61.0% [17.6], tubastatin A: 1.8% [40.8], vorinostat: 50.8% [65.6]) (chidamide vs. PCI 34051:

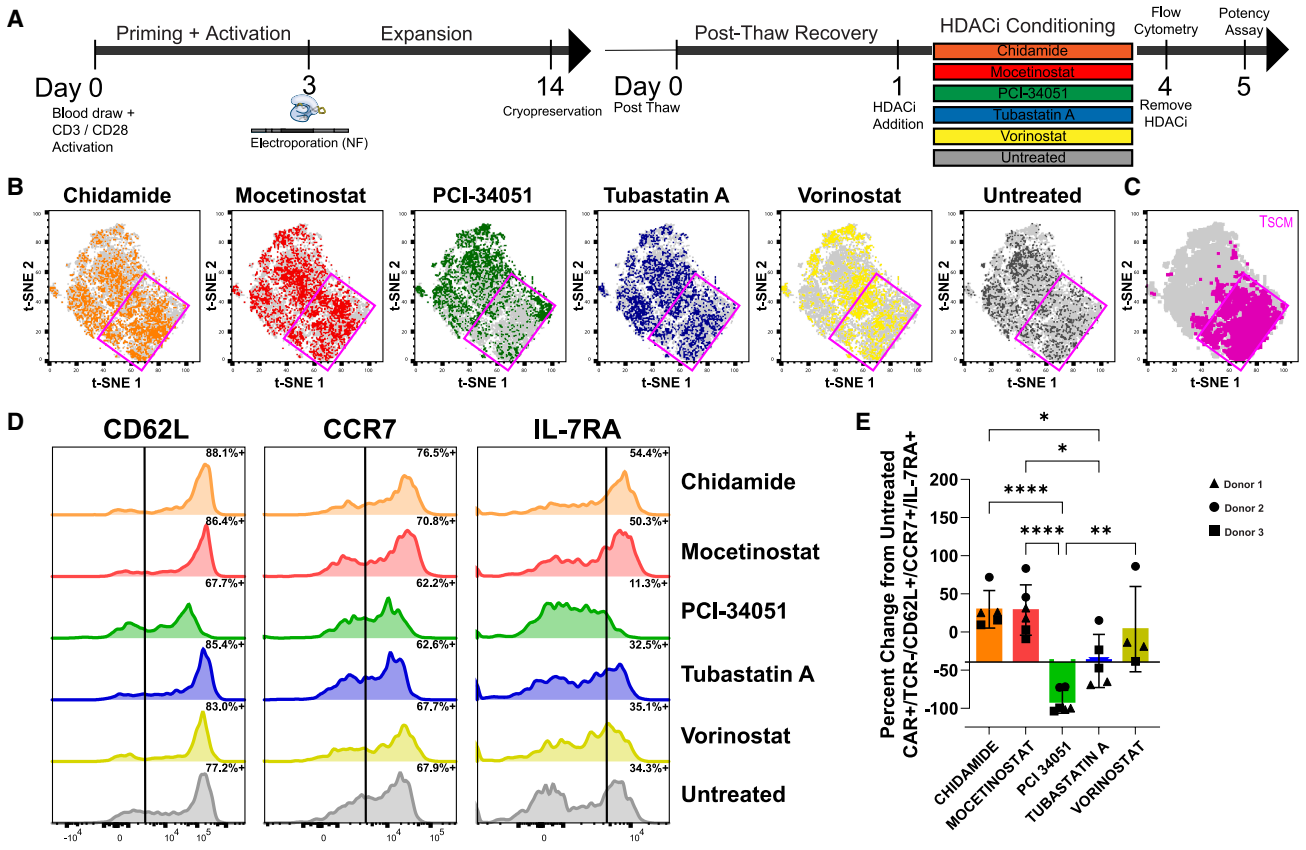

Figure 1. Chidamide or mocetinostat treatment enriches the stem cell memory (T_{SCM}) phenotype of GD2 *TRAC*-CAR T cells

(A) GD2 *TRAC*-CAR T cells were manufactured over the course of 14 days and cryopreserved. After thawed, they were rested for 24 h before treatment with HDACis for 72 h. (B) Marker expression t-SNE plots of GD2 *TRAC*-CAR T cells were treated with chidamide, mocetinostat, PCI-34051, tubastatin A, vorinostat, or vehicle (untreated). These plots were generated using flow cytometry data for expression of CD45RO, CD45RA, LAG3, PD-1, KLRG1, CD62L, CCR7, IL-7Rα, NKG2D, TRAIL, FASL, and HLA-DR on 500 Live/TCR^-/CAR^+ T cells from each analytical replicate. (C) t-SNE plot showing T_{SCM} ($CD62L^+$/$CCR7^+$/IL-$7R\alpha^+$) T cells and box containing most T_{SCM} (93%) for visualization. (D) Representative histograms of CD62L, CCR7, and IL-7Rα in HDACi-treated GD2 *TRAC*-CAR T cells showing the relative positive percentage for each marker within the bulk population. (E) Bar graph showing the percentage change in T_{SCM} ($CD62L^+$/$CCR7^+$/IL-$7R\alpha^+$) relative to untreated GD2 *TRAC*-CAR T cells for each HDACi-treated group. Three biological donors, $N_{Chidamide} = 5$ data points, $N_{Mocetinostat} = 5$ data points, $N_{PCI\text{-}34051} = 6$ data points, $N_{Tubastatin\ A} = 5$ data points, and $N_{Vorinostat} = 4$ data points. Error bar represents standard deviation. Statistical significance was determined with one-way ANOVA test using Dunnett's T3 test for multiple comparisons; $^*p < 0.05$, $^{**}p < 0.01$, $^{****}p < 0.0001$.

$p < 0.0001$, chidamide vs. tubastatin A: $p = 0.0303$, mocetinostat vs. PCI 34051: $p < 0.0001$, mocetinostat vs. tubastatin A: $p = 0.0245$, PCI 34051 vs. vorinostat: $p = 0.0019$). (Data are reported as mean [standard deviation]). Vorinostat modestly increased expression of these markers relative to PCI-34051, while tubastatin A and PCI-34051 decreased or did not affect such expression (Figures 1D and 1E). These trends appear predominantly driven by changes in IL-7Rα expression (Figure S5). As with third-generation GD2 *TRAC*-CAR T cells, we saw a similar enrichment of a T_{SCM} phenotype in second-generation PSMA *TRAC*-CAR T cells with a 4-1BB co-stimulatory domain, although the difference between the untreated and chidamide- or mocetinostat-treated CAR T cells was driven almost entirely by CD62L upregulation (Figure S6). Surprisingly, these results were accompanied by a decrease in β-catenin, suggesting an alternate pathway could explain T_{SCM} marker upregulation (Figure S7).

Additionally, chidamide and mocetinostat produced modest shifts in T cell subsets, increasing the proportion of cytotoxic ($CD8^+$) while decreasing helper ($CD4^+$) T cells (Figure S8A). Vorinostat slightly decreased helper T cells (Figure S8A). Chidamide and mocetinostat raised the proportion of effector-like ($CD45RO^-$/$CD45RA^+$) T cells without altering the central memory ($CD45RO^+$/$CD45RA^-$) population (Figure S8B). Exhaustion or anergy markers (PD-1, LAG3, and KLRG1) were unchanged following HDACi treatment (Figure S9).

HDACi-treated GD2 *TRAC*-CAR T cells retain their cytotoxicity against GD2-expressing NB cells *in vitro*

Given that phenotypical changes skewing toward a T_{SCM} phenotype in GD2 *TRAC*-CAR T cells can result in lower *in vitro* potency against NB,[14] we measured the cytotoxicity of HDACi-treated GD2 *TRAC*-CAR T cells during co-culture with the GD2-expressing

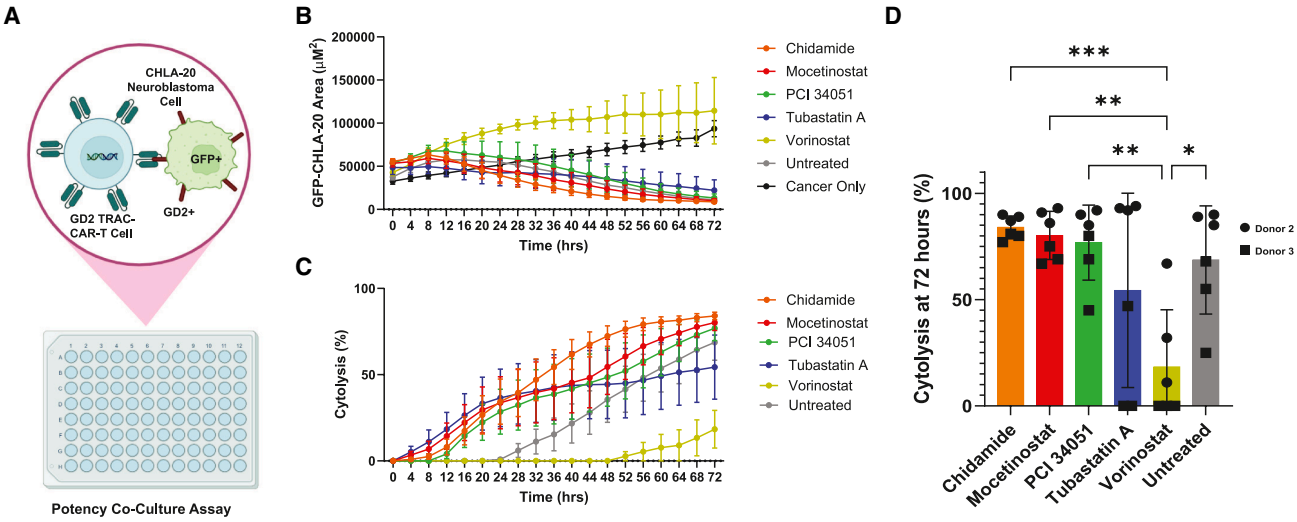

Figure 2. HDACi-treated GD2 *TRAC*-CAR T cells remain potent against GD2-expressing neuroblastoma CHLA-20 tumor

(A) GFP-expressing CHLA-20 cells were plated 24 h before adding the GD2 *TRAC*-CAR T cells treated with chidamide, mocetinostat, PCI-34051, tubastatin A, vorinostat, or vehicle (untreated) at a 10:1 effector-to-target ratio. GD2 *TRAC*-CAR T cell cytotoxicity was evaluated using the IncuCyte Live-Cell Analysis System. (B) GD2 *TRAC*-CAR T cell cytotoxicity was measured by tracking tumor fluorescence (GFP area: μm^2). (C) The percent cytolysis of CHLA-20 cells for each treatment group over time (hours). (D) Bar graphs depicting the percent cytolysis at 72 h for each treatment. Two donors, $N_{Chidamide} = N_{Mocetinostat} = N_{PCI\text{-}34051} = N_{Tubastatin\ A} = N_{Vorinostat} = N_{Untreated} = 6$ data points. Error bars represent mean and standard error of the mean (A, B, D, and E) or standard deviation (C and F). Statistical significance was determined with one-way ANOVA test using Dunnett's T3 test for multiple comparisons; $^{*}p < 0.05$, $^{**}p < 0.01$, $^{***}p < 0.001$.

NB cell line, CHLA20. To this end, GD2 *TRAC*-CAR T cells were treated for 72 h with chidamide, mocetinostat, PCI-34051, tubastatin A, vorinostat, or vehicle (untreated), after which HDACis were removed and rested in media for 24 h before they were added to co-cultures with GFP-expressing CHLA-20 cells at an effector-to-target (E:T) ratio of 10:1 (Figure 2A). The viability of tumor cells (CHLA-20) was measured for 72 h using the IncuCyte Live-Cell Analysis System as previously reported.[14,26,31,32] HDACi treatment had little effect on potency, except for vorinostat which markedly decreased cytolysis compared to all groups except for tubastatin A (chidamide: 84.0% [5.4], mocetinostat: 80.2% [11.3], PCI-34051: 76.8% [17.6], tubastatin A: 54.3% [45.7], vorinostat: 18.3% [26.9], and untreated: 68.7% [25.4]) (chidamide vs. vorinostat: $p = 0.0014$, mocetinostat vs. vorinostat: $p = 0.0029$, PCI 34051 vs. vorinostat: $p = 0.0052$, and vorinostat vs. untreated: $p = 0.0211$) (Figures 2B–2D). Next, we investigated the expression of two cytotoxic molecules, interferon gamma (IFN-γ) and perforin, in response to the CAR activation by the GD2 antigen. GD2 *TRAC*-CAR T cells treated with HDACi were co-cultured with CHLA-20 cells at a 5:1 E:T ratio for 24 h, and intracellular flow cytometry was performed on the HDACi-treated GD2 *TRAC*-CAR T cells. We observed similar IFN-γ and perforin expression across all HDACi-treated GD2 *TRAC*-CAR T cells except with mocetinostat-treated GD2 *TRAC*-CAR T cells that displayed an increase in perforin expression (Figure S10).

From our previous spectral flow cytometry analysis, we observed that ligands associated with CAR-independent killing pathways (NKG2D, TRAIL, and FasL) were significantly decreased after HDACi treatment (Figure S11). Notably, vorinostat produced the greatest reduction in TRAIL and NKG2D expression among the HDACis investigated (Figure S11). Given that chidamide and mocetinostat boosted the T_{SCM} without compromising GD2 *TRAC*-CAR T cell cytotoxicity, subsequent screening and analyses were limited to these HDACis.

The class I HDACis chidamide and mocetinostat have different impact on GD2 *TRAC*-CAR T cell lactate production

Both HDACi treatment and changes in stem cell memory phenotype can be accompanied by shifts in metabolism.[11,20,33] To assay for this, we collected media samples from thawed GD2 *TRAC*-CAR T cells after 72 h of HDACi treatment and measured the concentrations of glutamate, glutamine, lactate, and malate using high-throughput assays (Figure 3A). Given that improving the stem memory compartment in GD2 *TRAC*-CAR T cells can result in reduced lactate production, we anticipated that chidamide and mocetinostat will yield similar findings.[14] We normalized the concentrations of each metabolite to the vehicle (untreated) and expressed them as a percentage. Surprisingly, we saw chidamide did not affect lactate production while mocetinostat significantly reduced it, as evidenced by a nearly 50% decrease in lactate relative to chidamide (chidamide: 99.0% [26.9], mocetinostat: 52.2% [10.9]) (chidamide vs. mocetinostat: $p = 0.0031$) (Figure 3B). The production of malate, a key metabolite in the citric acid cycle, appeared to be decreased following mocetinostat treatment by approximately 12% (chidamide: 77.3% [12.6], mocetinostat: 64.6% [3.2]) (chidamide vs. mocetinostat: $p = 0.0212$)

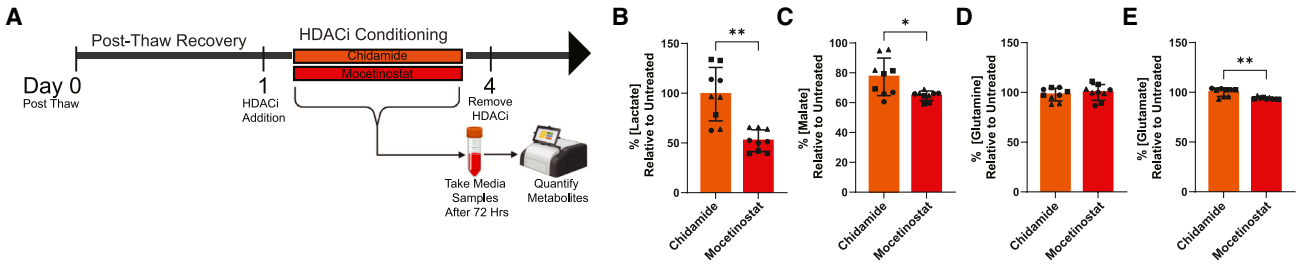

Figure 3. HDACi-treated *TRAC*-CAR T cells modulate various metabolite production

(A) Experimental scheme: thawed GD2 *TRAC*-CAR T cells were treated with chidamide, mocetinostat, or vehicle (untreated) for 72 h. The supernatant was collected, and the concentrations of various analytes including lactate, glucose, malate, glutamate, and glutamine were measured. Bar graphs depicting the percentage of metabolite in media relative to untreated samples for (B) lactate, (C) malate, (D) glutamine, or (E) glutamate for each condition. Three donors, $N_{Chidamide} = N_{Mocetinostat} = N_{Untreated} = 9$ data points. Error bar represents standard deviation. Statistical significance was determined with one-way ANOVA tests using Dunnett's T3 test for multiple comparisons; $^{*}p < 0.05$, $^{**}p < 0.01$.

(Figure 3C). Glutamine consumption (chidamide: 97.8% [6.3], mocetinostat: 100.0% [7.9]) was not significantly affected, while glutamate production (chidamide: 100.1% [4.1], mocetinostat: 94.0% [1.1]) (chidamide vs. mocetinostat: $p = 0.0056$) appeared slightly reduced by the mocetinostat treatments, albeit only by 6% (Figures 3C and 3D).

To complement the metabolite profiling, we measured oxygen consumption rate (OCR) using the Resipher Dynamic Oxygen Consumption Reader, which continuously monitors the oxygen in cell culture media over time, providing real-time metabolic information.[34] To this end, GD2 *TRAC*-CAR T cells (100,000 per well) were treated with chidamide or mocetinostat, and the OCR was monitored for 4 days in 96-well plates (Figure S12A). Mocetinostat significantly reduced OCR compared to untreated GD2 *TRAC*-CAR T cells, whereas chidamide had no effect (Figures S12B and S12C).

Chidamide and mocetinostat have diverging effects on mitochondrial morphology

Given that lactate and malate metabolism can correlate with mitochondrial function[35,36] and changes in T cell differentiation status can affect mitochondrial morphology,[37] we further investigated the morphology of mitochondria in the GD2 *TRAC*-CAR T cells following HDACi treatment. We used confocal microscopy to generate z stacks of GD2 *TRAC*-CAR T cell mitochondria stained with MitoTracker Red CMXRos. Z stacks were processed (ImageJ) to assess mitochondrial morphology features (Figure 4A) and ranked by importance using a permutation test (Figure S13). Chidamide and mocetinostat appeared to have opposite effects on the mitochondria where they induced a smaller/less branched and larger/more branched morphology, respectively, relative to untreated *TRAC* CAR T cells (Figure 4B). We then compared the top three most important features (total mitochondrial volume, total mitochondrial surface area, and total length of mitochondrial branches) and confirmed that chidamide induced a smaller, fragmented morphology, while mocetinostat had the opposite effect (chidamide: 26.0 μm^3 [20.0], mocetinostat: 43.5 μm^3 [25.0], untreated: 34.4 μm^3 [15.4]) (chidamide vs. mocetinostat: $p < 0.0001$, d = 0.37, chidamide vs. untreated: $p = 0.0044$, d = 0.49, mocetinostat vs. untreated: $p = 0.0019$, d = 0.21), surface area (chidamide: 113.2 μm^2 [80.6], mocetinostat: 174.5 μm^2 [100.7], untreated: 141.3 μm^2 [63.2]) (chidamide vs. mocetinostat: $p < 0.0001$, d = 0.31, chidamide vs. untreated: $p = 0.0238$, d = 0.40, mocetinostat vs. untreated: $p = 0.006$, d = 0.36), and branch length (chidamide: 34.5 µm [26.2], mocetinostat: 55.6 µm [35.3], untreated: 43.7 µm [23.3]) (Figure 4C). The number of mitochondria detected per cell (chidamide vs. mocetinostat: $p < 0.0001$, d = 0.30, chidamide vs. untreated: $p = 0.0368$, d = 0.38, mocetinostat vs. untreated: $p = 0.0243$, d = 0.19) (chidamide: 8.5 mitochondria [6.1], mocetinostat: 8.6 mitochondria [5.6], untreated: 8.0 mitochondria [5.2]) (chidamide vs. mocetinostat: d = 0.09; chidamide vs. untreated: d = 0.09; mocetinostat vs. untreated: d = 0.03) (Figure 4C) and mitochondrial mass assessed by flow cytometry (Figure S14) remained unchanged with HDACi treatment, indicating that the observed morphological changes were not due to the degradation or biogenesis of mitochondria.

To isolate the individual contribution of class I, IIb, and IV HDAC inhibition to the observed phenotype and morphological changes, we treated GD2 *TRAC*-CAR T cells with additional inhibitors, entinostat (HDAC1/2/3), DFK2 (HDAC10), or FT895 (HDAC11) (Tables S1 and S2). We assessed changes in stem-like markers following treatment with chidamide, mocetinostat, entinostat, DFK2, FT895, and various combinations of these inhibitors including entinostat + DFK2 and entinostat + FT895. Compared to untreated GD2 *TRAC*-CAR T cells, only class I inhibition increased stem-like marker expression (Figures S15A and S15B). We then compared the mitochondrial morphology of each treatment group and observed that chidamide, entinostat, and DFK2 consistently led to reduced mitochondrial surface area, volume, and total branch length (Figure S15C), suggesting both HDAC1/2/3 and HDAC10 contribute to the observed fragmentation.

Chidamide increases GD2 *TRAC*-CAR T cell persistence *in vivo*

Given that *in vitro* T_{SCM} phenotype changes, as well as shifts in metabolism and mitochondrial morphology can affect persistence, exhaustion, and memory formation *in vivo*,[11,38] we evaluated the

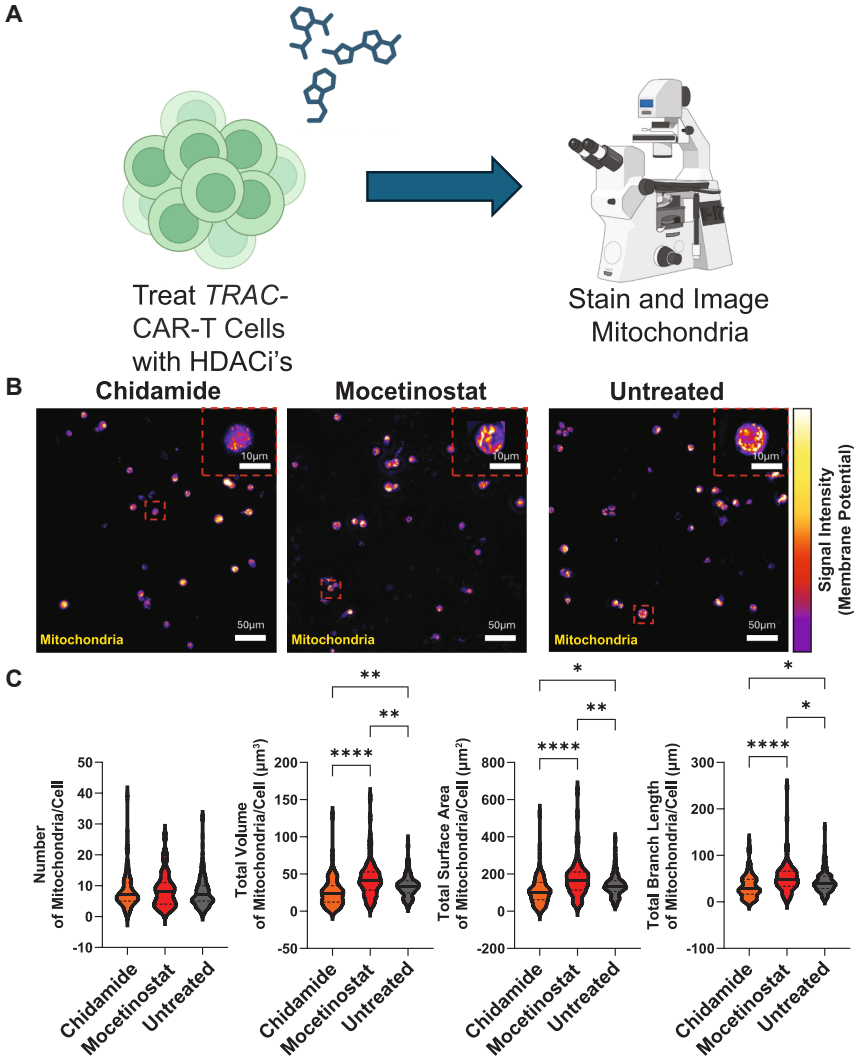

Figure 4. Chidamide and mocetinostat change mitochondrial morphology in GD2 *TRAC*-CAR T cells

(A) Experimental scheme: thawed GD2 *TRAC*-CAR T cells were treated with HDACi for 72 h and stained with MitoTracker Red CMXRos, imaged on a single-cell level, and analyzed using ImageJ. (B) Representative images of each HDACi treatment condition (chidamide, mocetinostat, or untreated). (C) Violin plot of the number of mitochondria in each single cell, the total volume, total surface area, and total branch length per cell for each HDACi treatment. Two donors, $N_{Chidamide}$ = 83, $N_{Mocetinostat}$ = 81, $N_{Untreated}$ = 161 data points. Error bars represent standard deviation. Statistical significance was determined with one-way ANOVA test using Dunnett's T3 test for multiple comparisons; $^{*}p < 0.05$, $^{**}p < 0.01$, $^{****}p < 0.0001$.

impact of the HDACi treatment (chidamide and mocetinostat) in a xenograft model of NB in NOD-*Rag1*^{null}*IL2rg*^{null} (NRG) mice. First, to further establish clinical relevance, we confirmed that chidamide and mocetinostat induce similar phenotypic changes in freshly manufactured, non-cryopreserved GD2 *TRAC*-CAR T cells (Figure S16). Then, 10 million luciferase-expressing GD2^{+} NB cells (CHLA-20) were subcutaneously implanted in NRG mice, and 5 days later they were randomized based on tumor bioluminescence into the treatment arms including (1) chidamide-treated, (2) mocetinostat-treated, and (3) vehicle (untreated) non-cryopreserved GD2 *TRAC*-CAR T cells freshly manufactured from T cells obtained from a healthy donor. Tumor-bearing mice were intravenously (i.v.) administered 1.5 million GD2 *TRAC*-CAR T cells treated with chidamide or mocetinostat or vehicle (untreated) prior to mice injection (Figure 5A). The GD2 *TRAC*-CAR T cells were treated with the HDACi for 72 h and rested for 48 h before i.v. administration. Tumor size was monitored through bioluminescence on days 0, 2, and 9 after GD2 *TRAC*-CAR T cell infusion. We subsequently observed no statistically significant difference in tumor size between the three treatment arms (chidamide: 2.9e7 photons/s/cm^2/sr [1.9e7], mocetinostat: 1.8e7 photons/s/cm^2/sr [1.4e7], untreated: 1.2e7 photons/s/cm^2/sr [7.5e6]) (Figures 5B and 5C), suggesting that GD2 *TRAC*-CAR T cells retain similar antitumor activity *in vivo* as observed with our *in vitro* data.

Nineteen days after the GD2 *TRAC*-CAR T cell infusion, the spleens were harvested, and the expression of memory, exhaustion, and lineage markers was analyzed by flow cytometry (Figure S17). To assess persistence, we quantified the number of overall T lymphocytes using the pan immune and T cell markers CD45 and CD5 and GD2 *TRAC*-CAR T cells by gating lymphocytes on CAR^{+}/TCR^{-} events in the spleen. We observed a 10- and 5.6-fold increase in CD45^{+}/CD5^{+} lymphocytes with chidamide treatment relative to mocetinostat (chidamide: 5,053 cells [6,330], mocetinostat: 503.4 cells [407.6], untreated: 905.2 cells [915.1]) (chidamide vs. mocetinostat: $p = 0.0094$, chidamide vs. untreated: $p = 0.047$) and untreated and a 14.8- and 11.1-fold increase in CAR^{+}/TCR^{-} lymphocytes with chidamide treatment relative to mocetinostat and untreated GD2 *TRAC*-CAR T cells (chidamide: 772 cells [1,127], mocetinostat: 52.3 cells [44.4], untreated: 69.4 cells [82.6]) (chidamide vs. mocetinostat: $p = 0.0218$, chidamide vs. untreated: $p = 0.0594$) (Figure 5D). Of note, chidamide enriched for both CD8^{+} (chidamide: 715 cells [1,073], mocetinostat: 41 cells [38], untreated: 40 cells [45]) (chidamide vs. mocetinostat: $p = 0.0241$) and CD4^{+} (chidamide: 57 cells [81], mocetinostat: 9 cells [9], untreated: 7 cells [7]) (chidamide vs. mocetinostat: $p = 0.0362$) *TRAC*-CAR T cells, but preferentially for CD8^{+} (Figure 5D). This coincided with a significant increase in CD8^{+} cytotoxic GD2

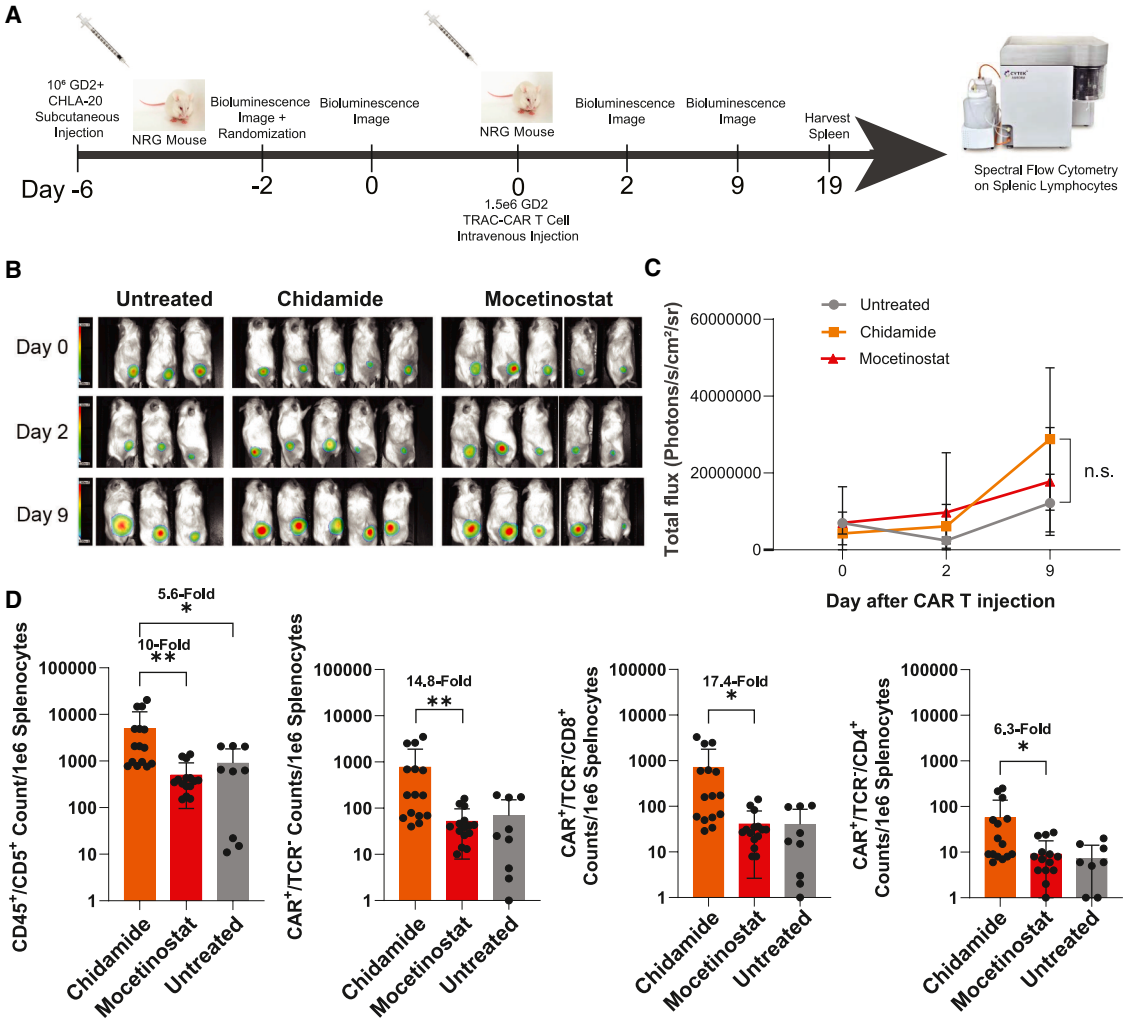

Figure 5. Chidamide enhances GD2 *TRAC*-CAR T cell persistence *in vivo*

(A) Experimental scheme: NRG mice were injected with CHLA-20 cells imaged, randomized, and injected with GD2 *TRAC*-CAR T cells treated with chidamide, mocetinostat, or non-treated, and imaged once per week. After 19 days, mouse spleens were isolated and stained with a spectral flow cytometry immunophenotype panel. (B) Representative bioluminescence images of mice treated with vehicle (untreated), chidamide-treated, and mocetinostat-treated GD2 *TRAC*-CAR T cells were taken on days 0, 2, and 9 post-CAR T cell injection. (C) Total tumor flux (p/s) for each treatment arm showing no statistical difference. (D) Bar graph depicting the percent of $CD45^+/CD5+$, $CD45^+/CD5^+/TCR^-/CAR^+$, $CD45^+/CD5^+/TCR^-/CAR^+/CD8^+$, and $CD45^+/CD5^+/TCR^-/CAR^+/CD4^+$ lymphocytes from isolated mouse spleens for mice treated with chidamide, mocetinostat or untreated GD2 *TRAC*-CAR T cells. One donor, $N_{Chidamide} = 5$, $N_{Mocetinostat} = 5$, $N_{Untreated} = 3$ mice measured in triplicate for persistence analysis. One donor, $N_{Chidamide} = 15$, $N_{Mocetinostat} = 12$, $N_{Untreated} = 9$ data points. Error bars represent standard deviation. Statistical significance was determined with one-way ANOVA test using Dunnett's T3 test for multiple comparisons; $^*p < 0.05$, $^{**}p < 0.01$.

TRAC-CAR T cells and subsequent decrease in $CD4^+$ within the bulk population following chidamide treatment relative to mocetinostat (Figure S18). These findings indicate that chidamide increased GD2 *TRAC*-CAR T cell persistence *in vivo*, with a preference for $CD8^+$ cells.

Chidamide enhances naive phenotype *in vivo* without inducing exhaustion

We next assessed T cell differentiation within live/$CD45^+/CD5^+/TCR^-/CAR^+$ splenic lymphocytes by constructing a reduced two-dimensional t-SNE space using the expression of CD45RO, CD45RA, LAG3, PD-1, KLRG1, CD39, TIM3, TIGIT, CD62L, CCR7, IL-7Rα, NKG2D, TRAIL, FASL, and HLA-DR in pooled samples of GD2 *TRAC*-CAR T cells isolated from spleens of chidamide-treated, mocetinostat-treated, and untreated GD2 *TRAC*-CAR T cells separated in the t-SNE space signaling potential differences in marker expression between the groups (Figure 6A). Samples separated visually into a left, top, and right group, where the left group, which defines the T_{SCM} ($CD62L^+/CCR7^+/IL\text{-}7R\alpha^+$) cells, was enriched for chidamide-treated GD2 *TRAC*-CAR T cells and the right

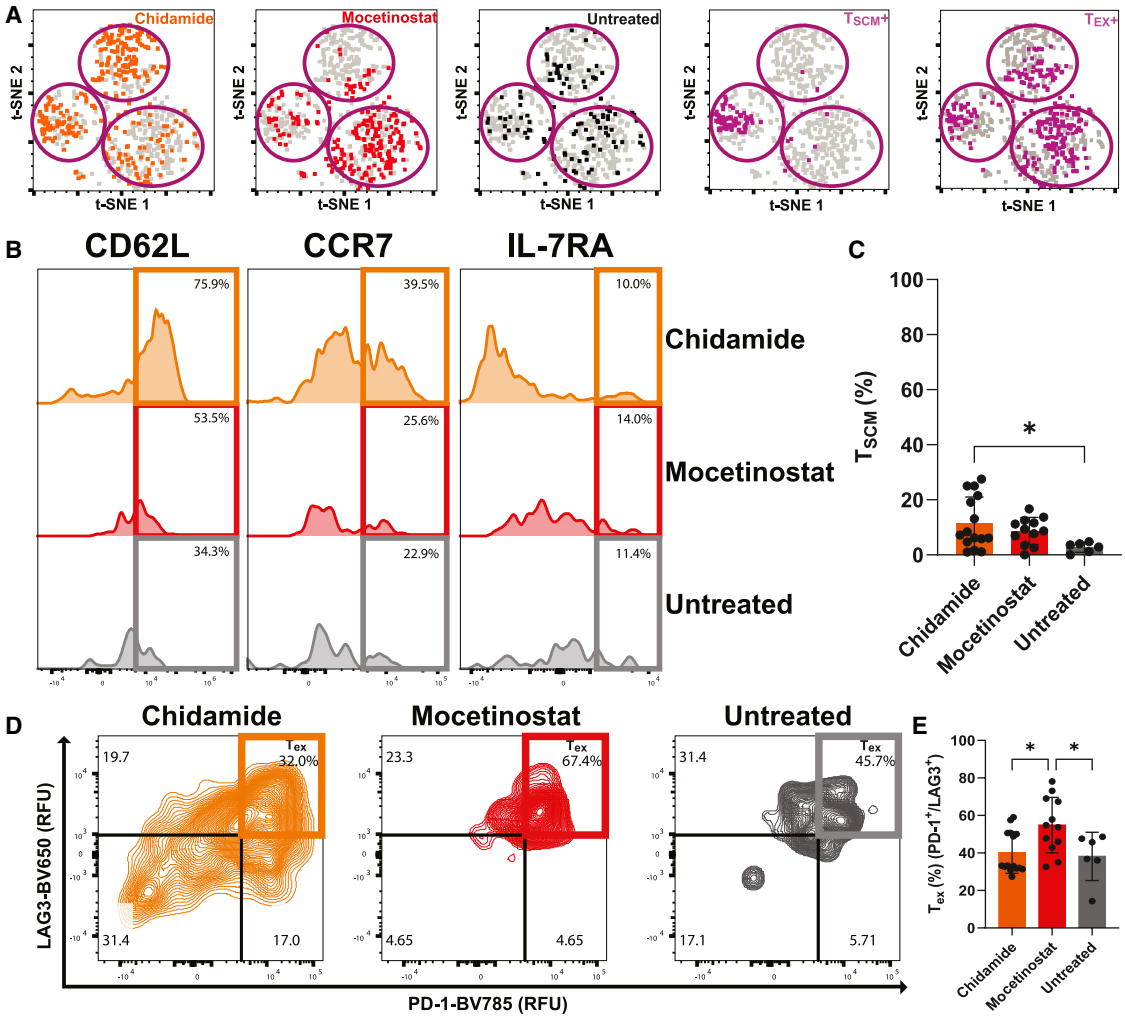

Figure 6. Chidamide enhances GD2 *TRAC*-CAR T cell naive phenotype and resistance to exhaustion *in vivo*

(A) Marker expression t-SNE plots of vehicle (untreated), chidamide-treated, and mocetinostat-treated GD2 *TRAC*-CAR T cells generated using flow cytometry data for expression of CD45RO, CD45RA, LAG3, PD-1, KLRG1, CD39, TIM3, TIGIT, CD62L, CCR7, IL-7Rα, NKG2D, TRAIL, FASL, and HLA-DR on Live/CD45$^+$/CD5$^+$/TCR$^-$/CAR$^+$ splenic lymphocytes. t-SNE shows separation for chidamide, mocetinostat, or Untreated GD2 *TRAC*-CAR T cells, T_{SCM} (stem cell memory: CCR7$^+$/CD62L$^+$/IL-7Rα$^+$) and T_{ex} (exhausted: PD-1$^+$/LAG3$^+$); (B) representative histograms of CD62L, CCR7, and IL-7Rα; and (C) bar graph showing percentage of T_{SCM} (CD62L$^+$/CCR7$^+$/IL-7Rα$^+$) for vehicle (untreated), chidamide-treated, mocetinostat-treated GD2 *TRAC*-CAR T cells. (D) Representative contour plots of vehicle (untreated), chidamide-treated, and Mocetinostat-treated GD2 *TRAC*-CAR T cells depicting PD-1 vs. LAG3 expression. (E) Bar graph of double-positive (PD-1$^+$LAG3$^+$) populations (T_{ex}). Populations with less than 20 events were omitted from phenotypic analysis. One donor, $N_{Chidamide}$ = 15, $N_{Mocetinostat}$ = 12, $N_{Untreated}$ = 6 data points. Error bars represent standard deviation. Statistical significance was determined with one-way ANOVA tests using Dunnett's T3 test for multiple comparisons; *$p < 0.05$.

group, defining mainly the exhausted T cells (T_{ex}: PD-1$^+$/LAG3$^+$), appeared enriched for mocetinostat-treated GD2 *TRAC*-CAR T cells (Figure 6A). Indeed, the fraction of T_{SCM} was the highest following chidamide treatment and was 4-fold higher than that of untreated GD2 *TRAC*-CAR T cells (chidamide: 11.6% [9.5], mocetinostat: 8.7% [4.9], untreated: 2.8% [1.8]) (chidamide vs. untreated: $p = 0.0417$) (Figures 6B and 6C), which appeared primarily driven by significantly higher CD62L and CCR7 but not IL-7Rα, as its expression was unchanged relative to untreated cells (Figure S19). Coinciding with the trends in t-SNE plots, mocetinostat treatment resulted in significantly more exhausted GD2 *TRAC*-CAR T cells than either chidamide or untreated GD2 *TRAC*-CAR T cells (chidamide: 40.1% [11.1], mocetinostat: 54.9% [14.8], untreated: 38.2% [12.9]) (chidamide vs. mocetinostat: $p = 0.0161$, mocetinostat vs. untreated: $p = 0.0371$) (Figures 6D and 6E). Specifically, mocetinostat treatment induced higher expression of PD-1, LAG3, and CD39 compared to chidamide treatment, while TIGIT and TIM3 expression remained unchanged (Figure S20). Chidamide treatment alone induced significantly higher expression of KLRG1 (Figure S20C). An increase in stem cell memory phenotype in *TRAC*-CAR T cells

can translate to an enriched central memory phenotype *in vivo*.[14] However, we observed that CD45RA and CD45RO expression was virtually unchanged by HDACi treatment, with more cells occupying a memory-like ($CD45RO^+/CD45RA^-$) than effector-like ($CD45RO^-/CD45RA^+$) state (Figure S21). We also analyzed the expression of receptors for CAR-independent killing pathways and the late-stage activation marker HLA-DR. The expression of TRAIL, NKG2D, and HLA-DR was unchanged with HDACi treatment (Figure S22). However, we noted a significant decrease in Fas ligand expression with chidamide treatment relative to other conditions (Figure S22).

To determine how chronic stimulation in the short term could lead to these observed differences, we subsequently investigated the response of GD2 *TRAC*-CAR T cells treated with HDACis to serial stimulation by CHLA-20 NB cells. HDACi-treated GD2 *TRAC*-CAR T cells and CHLA-20 cells were added to 12-well plates in a 2:1 E:T ratio, with additional CHLA-20 cells added every 2–3 days. Ten days after the initiation of the co-culture, the expression of memory and exhaustion markers was assessed by spectral flow cytometry (Figure S23). We observed a greater retention of an effector-like population, a reduction in central memory-like cells, and a more naive T cells phenotype with mocetinostat treatment, while there was little difference in the exhaustion markers (Figure S24).

DISCUSSION

We used a class selective HDAC inhibitor, chidamide (class I/IIb), to enhance the function and the T_{SCM} phenotype of GD2 *TRAC*-CAR T cells. The incorporation of this small molecule in the manufacturing process yielded an improved pre-infusion CAR T cell product without adding complexity and prolonging their manufacture. Unlike prior studies using virally engineered CAR T cells,[20] our approach utilized CRISPR-Cas9-mediated insertion of a 3.7 kb HDR template into the *TRAC* locus, enabling evaluation of HDACi effects in a non-viral context. The transient disruption of HDAC1/2/3/10 (with chidamide) promoted the expression of T_{SCM} surface markers while enhancing *in vivo* persistence compared to untreated GD2 *TRAC*-CAR T cells.

Across multiple HDACis evaluated (Table S1), chidamide and mocetinostat significantly increased the proportion of $CD62L^+/CCR7^+/IL\text{-}7R\alpha^+$ cells by over 75%, indicating a pronounced shift toward a T_{SCM}-like phenotype (Figure 1). The isoform selectivity of these two HDACis suggests that the observed phenotypic shifts might be due to the targeted modulation of HDAC 1, 2, 3, 10, or 11. This finding was corroborated by a similar rise in CD62L in a second-generation PSMA *TRAC*-CAR T cells with a 4-1BB co-stimulatory domain (Figure S6). Although we do not observe an increase in CCR7 and IL-7Rα, the increase in CD62L may be sufficient to support our findings, since CD62L is arguably considered a more stable indicator of a transition toward a stem-like phenotype.[11,39] These align with a previous report showing elevated CD62L expression, with virally manufactured GD2 CAR T cells following treatment with class I HDACis such as chidamide and M344.[20] These changes coincided with reduced exhaustion, enhanced potency *in vitro* and *in vivo*, and improved persistence driven by an increase in Wnt/β-catenin signaling and histone acetylation (H3K27ac, H3ac, and H4ac).[20] By contrast, we observed a reduced β-catenin expression following class I HDACi treatment, suggesting that the increase in stem memory surface markers arises via an alternate pathway (Figure S7). Chidamide has been observed to inhibit Wnt/β-catenin signaling via MYCN inhibition and DKK3 upregulation in lymphomas.[40–42] Thus, it is possible that chidamide simply downregulated β-catenin levels through the aforementioned mechanism. In the absence of β-catenin to stabilize TCF1/LEF-1 complexes, they can still regulate target genes through alternative binding factors such as ATF2 or ALY,[43,44] which is likely aided by the increased transcriptional access of stem-like genes like *SELL* and *CCR7*.[20] Notably, chidamide or mocetinostat treatment did not further downregulate exhaustion surface markers (PD-1 or LAG3) likely because CRISPR-engineered *TRAC*-CAR T cells already exhibit reduced levels of them *in vitro* and *in vivo* compared to virally manufactured cells[14,26] (Figure S9).

Stem-like GD2 *TRAC*-CAR T cells have previously shown a reduced potency against the $GD2^+$ NB cell line, CHLA-20,[26] which also coincided with an increase in CD62L/CCR7 expression.[14] Chidamide or mocetinostat treatment did not significantly impact cytotoxicity, only vorinostat did (Figure 2). This impairment may reflect the downregulation of alternative cytotoxic pathways such as NKG2D, TRAIL, or FasL (Figure S11) and/or vorinostat's known inhibition of ZAP70 and AKT phosphorylation, which are crucial for effective CAR signaling.[45] Notably, mocetinostat uniquely increased perforin (Figure S10), yet reduced lactate secretion, malate, and oxygen consumption may suggest insufficient metabolic support for sustained cytotoxicity, yielding a net neutral effect on CAR T cell potency (Figures 3 and S12). These findings contrast prior reports that class I HDAC inhibition enhances cytotoxic function and upregulates cytotoxic genes such as *GZMB*, *IFNG*, and *CD8a*.[20]

Chidamide markedly remodeled mitochondrial morphology toward a more fragmented phenotype (Figure 4). Smaller, less-branched mitochondria can be an indicator of increased capacity for glycolysis and mitophagy, which could provide the metabolic machinery for a rapid transition into an effector-like upon repeated antigen stimulation.[37,38] *In vivo*, chidamide increased the absolute numbers of total CAR^+, $CD8^+$, and $CD4^+$ T cells and upregulated KLRG1 compared to mocetinostat or untreated GD2 *TRAC*-CAR T cells (Figure 6). KLRG1 can indicate terminal effector differentiation (Figure S20),[46–48] which can explain the increased burst in proliferation with chidamide. However, it may eventually limit proliferation in highly differentiated subsets,[49,50] especially in NB that can overexpress one of its ligands, N-cadherin, a likely reason for the lack of improved potency *in vivo* or *in vitro*.[51,52] The increase in GD2 *TRAC*-CAR T cell number following chidamide treatment may be due to the reduction of FasL expression, limiting Fas/FasL-mediated fratricide killing and improving persistence.[53] Although PD-1, LAG3, and CD39 were

expressed across all treatment groups *in vivo*, mocetinostat induced the highest levels (Figures 6 and S20), possibly due to metabolic dysfunction (reduced lactate secretion and oxygen consumption). Persistent T cell subsets expressing PD-1 and LAG3 that have been observed in patients with acute lymphoblastic leukemia (ALL) can last for more than 18 years,[54] suggesting these factors alone do not indicate dysfunction. Given the downregulation of T_{SCM} markers *in vivo* from T cell differentiation, *in vivo* intervention with chidamide could restore a naive phenotype while reducing exhaustion as seen previously.[20] Furthermore, chidamide, in combination with GD2 *TRAC*-CAR T cells, could remodel the solid TME by modulating cancer metabolism and immunosuppressive cell types.[55–57]

Although pre-treatment with chidamide increases T_{SCM} markers and persistence *in vivo*, it targets multiple isoforms, making it difficult to unequivocally determine whether the observed effects are attributable specifically to class I HDACs (HDAC1/2/3) or HDAC10 or if they involve cooperative activity between these isoforms. We subsequently tested entinostat, a class I (HDAC1/2/3) HDACi, and DFK2, a HDAC10 inhibitor, and observed that class I (HDAC1/2/3) inhibition drove the increase in T_{SCM} surface markers, whereas mitochondrial fragmentation was due to the combination of HDAC1/2/3 and HDAC10 (Figure S15). The divergent effects of chidamide and mocetinostat may stem from their selective inhibition of HDAC10 and HDAC11, respectively. HDAC11 inhibition has been linked to increased mitochondrial content and enhanced fatty acid oxidation,[58] while HDAC10 inhibition disrupts autophagosomes and lysosome fusion, reducing autophagy, damaging mitochondria, and increasing ROS levels.[59] Mitochondrial health is essential for CAR T cell infiltration in the TME, persistence, and effector function.[37,38,60,61] Therefore, it is possible that the short-term HDAC10 inhibition ensuing from chidamide, might lead to mitochondrial damage due to impaired autophagy, with the subsequent recovery or compensatory mechanism promoting the formation of newer and healthier mitochondria with improved performance, possibly via mitophagy.[62] Additionally, while reduced autophagy is known to cause cellular dysfunction in T cells,[63,64] transient autophagy inhibition can actually reduce exhaustion, delay differentiation, and shift cells toward glycolysis.[65]

Most experiments utilized cryopreserved GD2 *TRAC*-CAR T cells, which may confound metabolic and mitochondrial morphology analyses. However, fresh non-cryopreserved GD2 *TRAC*-CAR T cells from a healthy donor were used for *in vivo* studies, where upregulation of stem cell memory markers was confirmed. Although the GD2 *TRAC*-CAR T cells were treated with chidamide for 72 h, shorter exposure produced similar shifts in T_{SCM} surface markers (Figures S25 and S26). For clinical integration, at least 24 h *ex vivo* treatment with chidamide may be needed with product release based on the upregulation of CD62L, CCR7, and/or IL-7Rα^+. Ultimately, these data suggest that chidamide can promote a T_{SCM} phenotype potentially independent of the Wnt/β-catenin signaling pathway and may ameliorate the manufacturing of CRISPR-engineered CAR T cells for NB and also adult solid tumors.

MATERIALS AND METHODS

Cell lines

The human GD2+ tumor cell line CHLA-20 (NB) was provided by M. Otto (University of Wisconsin-Madison). These cells were cultured in Dulbecco's modified Eagle's medium (DMEM) with high glucose (Gibco, Thermo Fisher Scientific, Waltham, MA), supplemented with 10% fetal bovine serum (FBS) (Avantor, Randor, PA) and 1% penicillin-streptomycin (Gibco, Thermo Fisher Scientific, Waltham, MA). Tumor cell lines were lentivirally transduced with AkaLUC-GFP (VectorBuilder, Chicago, IL). All cells were maintained at 37°C in a 5% CO_2 atmosphere. Cell line authentication was performed using genomic short tandem repeat analysis (IDEXX BioAnalytics Westbrook, ME) and morphological assessment according to American Type Culture Collection guidelines. *Mycoplasma* contamination was routinely checked using the Mycoplasma Detection Kit MycoStrip (InvivoGen, San Diego, CA).

CCK-8 cell counting assay

Two hundred thousand thawed GD2 *TRAC*-CAR T cells were plated in 96-well round bottom plates and treated with HDACis for 72 h. A CCK-8 (cell counting kit 8, Catalog No. GK10001, GLPBIO, Montclair, CA) was used to count cells according to the manufacturer's instructions.

Isolation of T cells and GD2 *TRAC*-CAR T cell manufacturing

T cells were isolated from leukocyte reduction system cones obtained from the Oklahoma Blood Institute (Oklahoma City, OK) using negative selection with the EasySep Human T Cell Isolation Kit (cat. no. 17951; STEMCELL Technologies, Vancouver, Canada). Alternatively, T cells were isolated from peripheral blood of healthy donors under a University of Wisconsin-Madison institutional review board-approved protocol (2017-1070 and 2019-0865) using the RosetteSep Human T Cell Enrichment Cocktail (cat. nos. 15021 and 15061; STEMCELL Technologies, Vancouver, Canada). The sequence for a third-generation GD2-CD28-OX40-CD3ζ construct was provided by M. Brenner (Baylor College of Medicine). GD2 *TRAC*-CAR T cells were manufactured by nucleofection or electroporation of CRISPR/Cas9 (no. 9212–0.25MG, Aldevron, Madison, WI) and Nanoplasmid HDR (Aldevron, Fargo, ND) templates into isolated T cells with the 4D Nucleofector X unit (cat. no. V4XP-3032, Lonza, Walkersville, VA) using pulse code EO-210 or the CTS Xenon Electroporation System (Thermo Fisher Scientific, Waltham, MA) using one pulse at 1,720 V with a width of 20 ms and cultured in ImmunoCult-XF T Cell Expansion Medium (cat. no. 10981; STEMCELL Technologies. Vancouver, Canada) supplemented with interleukin-7 (IL-7) (10 ng/mL; cat. no. 207-IL-005/CF; Bio-Techne, Minneapolis, MN) and IL-15 (10 ng/mL; cat. no. 247-ILB-005/CF; Bio-Techne, Minneapolis, MN) and maintained at 37°C in 5% CO_2 as previously described.[14,31] CAR T cells were frozen at 50e6 vials in 1.5 mL cryovials in CryoStor CS10 (cat. No. 100-1061, StemCell, Vancouver, Canada).

Flow cytometry analysis

CAR was detected using a 1A7 anti-14G2A antibody (National Cancer Institute, Biological Resources Branch, Bethesda, Maryland) and

conjugated to APC using a Lightning Link APC Antibody Labeling kit (cat. no. 705-0010, Novus Biologicals, Centennial, CO). TCR was detected using an anti-human TCR α/β antibody conjugated to BV421 (Cat No 306722, BioLegend, San Diego, CA). Flow cytometry to assess CAR and TCR positivity was performed on day 8 of manufacturing on an Attune NxT flow cytometer (Thermo Fisher Scientific, Waltham, MA). Immunophenotyping of cells was performed immediately following HDAC inhibitor treatment of CAR T cells using a spectral immunophenotyping panel on an Aurora spectral cytometer (Cytek, Fremont, CA). In brief, cells were plated in a 96-well round bottom plate (100k for CAR/TCR and 250k for spectral immunophenotyping), washed with 200 μL of PBS, and spun at 1,200 × *g* for 1 min, twice. Cells were then stained for viability with GhostRed 780 (cat. no. 50-105-2988, Tonbo Biosciences, San Diego, CA) or Live-Dead Blue (cat. no. L23105, Thermo Fisher Scientific, Waltham, MA). For CAR/TCR staining, 1 μL of GhostRed 780 was added to 10 mL of PBS to make a stock solution, and 100 μL of stock solution was added to each sample and incubated for 30 min in the dark. For spectral flow staining, Live-Dead Blue stain was resuspended in 50 μL of DMSO, 1 μL added per 1 mL PBS to make a stock solution, and 200 μL of stock solution added to each sample and incubated for 30 min in the dark. After viability staining, samples were washed twice and blocked for 30 min with 50 μL FACS buffer (0.5% BSA in PBS) with TruStain FcX solution (0.5 μL/sample) (cat. no. 422301, BioLegend, San Diego, CA). Antibodies were then added to 100 μL of FACS Buffer at the optimized amounts found in Table S2 and incubated for 1 h. Cells were then washed, resuspended in 200 or 75 μL of FACS buffer, and analyzed on the Attune or Aurora, respectively. For spectral immunophenotyping, we used CD4, CD8, TCR, and CAR positivity to define populations, and for all markers cells were gated by relative size, shape, singlets, viability, TCR negativity, and CAR transgene positivity to find an analyzable population of viable CAR T cells. All antibodies are listed in Table S2.

In vitro CAR T cell cytotoxicity assay

A total of 5,000 CHLA-20 cells expressing GFP and luciferase (AkaLUC-GFP-CHLA-20) were seeded in triplicate on 96-well plates and incubated for 24 h at 37°C. Twenty-four hours later, 100,000 thawed CAR^+ T cells, treated with or without HDAC inhibitors and rested for 24 h, were added to each well for an E:T ratio of 10:1. The plate was centrifuged for 5 min at 100 × *g* and then placed in the IncuCyte S3 Live-Cell Analysis System (Sartorius, Göttingen, Germany) and stored at 37°C, 5% CO_2. Images were taken every 4 h for 72 h. Green object area was used to calculate the relative amount of GFP^+ cancer cells in each well, and fluorescent images were analyzed using the IncuCyte Base Analysis Software. The percent cytolysis was calculated by the percent change in green object area relative to initial time point at the beginning of the assay.

In vivo human xenograft study in NRG mice

All animal experiments were approved by the University of Wisconsin-Madison Animal Care and Use Committee (ACUC protocol M006815). Male and female NOD-*Rag1*^{null}*IL2rg*^{null} (NRG) mice (9–12 weeks old; Jackson Laboratory, Bar Harbor, ME) were subcutaneously injected with 10 million AkaLUC-GFP CHLA-20 $GD2^+$ human NB cells in the flank to establish tumors. After 4 days, tumor engraftment was verified using bioluminescence measurements on the Lago In Vivo Imaging System (Spectral Instruments Imaging, Tuscon, AZ), the mice randomized, and baseline tumor measurements taken again on day 0. Then, 1.5 million CAR^+ T cells from day 23 of manufacturing were injected into the tail vein of each mouse. Mice were imaged on the Lago every 7 days after being sedated with isoflurane and intraperitoneal injections of ∼100 μL/mouse at 1.25 mM AkaLumine (cat. no. 305AKA, MediLumine, Montreal, Canada). To quantify the total flux in images, a region of interest was drawn around established tumors on day 0 and calculated by Aura In Vivo Imaging Software (Spectral Instruments Imaging, Tuscon, AZ). The total flux was calculated as the number of photons emitted per second, per square centimeter of surface area, into each steradian (photons/s/cm^2/sr). The minimum flux value was subtracted from each image to normalize for background signal.

Flow cytometry staining of splenic lymphocytes

Spleens were removed, mechanically dissociated, and filtered using a Corning 70 μM cell strainer. Suspensions were centrifuged for 10 min at 400 × *g*, and red blood cell (RBC) lysis was performed with ACK lysing buffer (Lonza, Walkersville, VA) for 3 min. The cells were then washed with PBS, centrifuged for 10 min at 400 × *g*, and resuspended in 1 mL of PBS. Cells were counted using trypan blue exclusion on the Countess II FL Automated Cell Counter. A total of 1 × 10^6 total cells was then added to 96-well round bottom plates and stained for a spectral immunophenotyping panel for analysis on an Aurora spectral cytometer (Cytek). In brief, samples were washed with PBS, stained with Live-Dead Blue for 30 min, blocked with FACS buffer and TruStain FcX, and incubated with the spectral immunophenotyping panel overnight at 4°C. For spectral immunophenotyping, we used CD4, CD8, TCR, and CAR positivity to define populations, and for all markers, cells were gated by relative size, shape, singlets, viability, CD5 positivity, CD45 positivity, TCR negativity, and CAR transgene positivity to find an analyzable population of viable CAR T cells. All antibodies and amounts are listed in Table S2.

In vitro serial stimulation and flow cytometry analysis of GD2 *TRAC*-CAR T cells

Forty thousand CHLA-20 cells were added to 12-well plates; 80,000 thawed CAR^+ T cells were seeded and then incubated at 37°C, 5% CO_2. A total of 80,000 CHLA-20 cells were added every 2–3 days for up to 10 days when the wells were harvested and stained for flow spectral cytometry. In brief, 300,000 CHLA-20/CAR T cells were washed with PBS, stained with Live-Dead Blue for 30 min, blocked with FACS buffer and TruStain FcX, and incubated with the spectral immunophenotyping for 1 h. For spectral immunophenotyping, we used TCR negativity to define populations, and for all markers, cells were gated by relative size, shape, singlets, viability, CD5 positivity, CD45 positivity, and TCR negativity to find an

analyzable population of viable T cells. All antibodies and amounts are listed in Table S2.

In vitro intracellular cytokine analysis

GD2 *TRAC*-CAR T cells were stimulated with CHLA-20 NB cells using a 5:1 E:T ratio for 24 h (5,000 CHLA-20 cells and 50,000 CAR^+), after which they were harvested for flow cytometry for internal expression of cytokines. Briefly, cells were treated with BD GolgiPlug Protein Transport Inhibitor (Containing Brefeldin A) (1 μL/mL) (cat. no. 555029, BD Bioscience, San Jose, CA) for 4–6 h prior to staining. Three hundred thousand CAR T/CHLA-20 cells were then added to a 96-well round bottom plate, washed with PBS, stained with Live-Dead Blue for 30 min, blocked with FACS buffer and TruStain FcX, treated with the BD Cytofix/Cytoperm Fixation/Permeabilization Kit (cat. no. 554714, BD Bioscience, San Jose, CA) according to the manufacturer's instructions, and incubated with anti-TCR, CD45, IFN-γ, and perforin antibodies (Table S2) for 1 h.

Mitochondrial staining

The mitochondrial mass of GD2 *TRAC*-CAR T cells was measured by performing flow cytometry on cells stained with MitoTracker Red CMXRos (ref. 9082; Cell Signaling Technology, Danvers, MA, USA). In brief, cells were stained with a stock solution of PBS containing 0.01 μL/mL of MitoTracker Red CMXRos (200 μL per sample of 250,000 T cells) for 20 min at 37°C, washed, and resuspended in 75 μL of FACS buffer (0.5% BSA in PBS).

Metabolite analysis

GD2 *TRAC*-CAR T cells were frozen on day 14 of manufacturing, subsequently thawed overnight, and then treated with HDAC inhibitors for 3 days prior to analysis. Supernatants were collected, acid-treated, and neutralized to quench endogenous dehydrogenase activity, then diluted in PBS per the manufacturer's instructions. Lactate, malate, glutamine, and glutamate levels were measured using Lactate-Glo, Malate-Glo, and Glutamine/Glutamate-Glo (cat. nos. J6021, J5021, JE9100, and J8021; Promega, Madison, WI), respectively. For each donor, inhibitor-treated samples were expressed relative to the matched untreated condition (percentage of untreated control).

Spectral flow cytometry data analysis

Analysis of spectral flow cytometry data was performed using Cytek's SpectroFlo program, Single positive controls for each color were collected and analyzed in SpectroFlo for positive and negative populations. SpectroFlo's unmixing algorithm was then used to compensate for spillover and autofluorescence of cells. Data were then exported to FlowJo (v.10.10.0), where samples were gated for non-debris, singlets, live cells, and downstream lineage markers. Median fluorescent intensity for each sample was calculated and input into Excel. Representative plots were generated in FlowJo using fluorescence minus one control to set positive gates.

Mitochondria staining and morphology analysis

Cells were stained using MitoTracker Red CMXRos (Ref: 9082; Cell Signaling Technology, Danvers, MA, USA) according to manufacturer's protocol. A 1 mM stock solution was prepared by reconstitution in 94.1 μL of DMSO. Cells were incubated in a 50 nM working solution diluted in PBS for 30 min at 37°C and 5% CO_2. Cells were washed twice with PBS and then plated in a glass bottom 96-well plate (ref: 165306; Thermo Fisher Scientific) imaging via Thunder Imager (Leica DMi8). Images were analyzed using the Mitochondria Analyzer plugin in FIJI.

Oxygen consumption in culture

We continuously detected the oxygen consumption of *TRAC* CAR T cells using the Resipher Platform (Lucid Scientific, Atlanta, GA). Briefly, 100,000 T cells were added to a standard 96-well plate in 200 μL of culture media. The lid was replaced with the Resipher sensing lid that contains an individual oxygen sensor for each well. The sensor continuously scans the media above cells to calculate the vertical oxygen gradient. The Resipher optical sensor magnetically attaches to the single-use lid that exports data to a local hub and then the cloud for the analysis. We scanned the media every 4 h and generated oxygen consumption curves.

Western blot

Cells from two different donors were treated with HDAC inhibitors at a concentration of 1 μM (chidamide, mocetinostat, or entinostat) or 10 μM (DFK2 or FT895) for 72 h and subsequently lysed using lysis buffer as previously described.[66] Protein concentrations were determined using the Bio-Rad Protein Assay Reagent (cat. no. 5000006 Bio-Rad Laboratories, Hercules, CA, USA), and 80 μg of total protein was loaded onto SDS-PAGE gels. Proteins were then transferred to PVDF membranes using the iBlot 3 system (Thermo Fisher Scientific, Waltham, MA, USA). Membranes were incubated overnight at 4°C with the appropriate primary antibodies, washed three times, and then incubated with the corresponding secondary antibodies for 1 h at room temperature. Chemiluminescent signals were detected using Western ECL Substrate (cat. no. 1705060, Bio-Rad Laboratories) and visualized with the Azure Biosystems imaging system (Dublin, CA, USA). Densitometry was performed using ImageJ (National Institutes of Health, Bethesda, MD, USA).

Data analysis and software

All data analyses were performed in GraphPad Prism (v.10.0.2) and Microsoft Excel. Statistical tests were done in GraphPad Prism and indicated in the figure legends. Nanoplasmid sequences were designed in Benchling. FlowJo was used to analyze .fcs files exported from SpectroFlo and Attune NxT software. Representative flow plots were exported from FlowJo. t-SNE plots were created using the DownSample plugin from FlowJo to select for and cluster pooled data in a concatenated .fcs file. Figures were created and organized using Adobe Illustrator (v.28.0). A p value less than 0.05 was defined as significant. Cohen's effect size was calculated by dividing the difference between treated and control group means and dividing by the pooled standard deviation of them. Data are presented as mean [standard deviation] in the text.

DATA AND CODE AVAILABILITY

Data are available upon reasonable request.

ACKNOWLEDGMENTS

We thank members of the Capitini, Ayuso, and Sodji labs for helpful discussion and comments on the manuscript. We also thank the University of Wisconsin (UW) Carbone Cancer Center Small Animal Imaging and Radiotherapy facility and Flow Cytometry Laboratory (supported by NIH P30 CA014520 and NIH S10 OD025225). We thank Abhay Kumar, Tom Foti, Tyler Kozisek, Reddy Seshidar Police, Denis Arutynov, Basam Barkho, and Patrick Paez from Aldevron for technical support with Cas9 proteins and Nanoplasmid vector preparation, Promega for support on media sample analysis, ScaleReady for technical support on the G-Rex system, and Thermo Fisher Scientific for support on optimization of EP on the CTS Xenon system. The contents of this article do not necessarily reflect the views or policies of the Department of Health and Human Services nor does mention of trade names, commercial products, or organizations imply endorsement by the US Government. This work was supported by the following: National Institutes of Health grant K08 CA285941 (to Q.H.S.), Centennial Scholar Fund UWSMPH (Q.H.S.), National Institutes of Health grant UL1TR002373, National Institutes of Health grant P30 CA014520 (UWCCC shared research services), and EBRP.

AUTHOR CONTRIBUTIONS

D.C. and A.S. optimized EP protocols, isolated and cultured T cells, performed virus-free transfections, and cryopreserved GD2 *TRAC*-CAR T cells. D.C. and V.G. performed *in vitro* co-culture experiments using cell culture techniques. D.C. performed flow cytometry. M.T. conducted *in vivo* experiments with support from Q.H.S. and D.C. Q.H.S. isolated mouse spleens/tumors, and D.C. performed flow cytometry. J.V., A.L., and K. Sylvester performed analysis of metabolites in media. S.Z. imaged and analyzed mitochondrial data. K. Saha provided GD2 CAR sequence and template. D.C. wrote the manuscript with input from all authors. D.C., M.T., S.Z., A.S., J.V., A.L., K. Sylvester, V.G., and Q.H.S. performed experiments and analyzed the data. J.A. and Q.H.S. supervised the research.

DECLARATION OF INTERESTS

D.C. and K. Saha are inventors on patents related to this work. K. Saha receives honoraria for advisory board membership for Andson Biotech and Bharat Biotech. All other authors declare that they have no competing interests.

SUPPLEMENTAL INFORMATION

Supplemental information can be found online at https://doi.org/10.1016/j.omton.2026.201200.

REFERENCES

1. Khan, A.N., Asija, S., Pendhari, J., and Purwar, R. (2024). CAR-T cell therapy in hematological malignancies: Where are we now and where are we heading for? Eur. J. Haematol. *112*, 6–18.
2. Liu, Y., An, L., Huang, R., Xiong, J., Yang, H., Wang, X., and Zhang, X. (2022). Strategies to enhance CAR-T persistence. Biomark. Res. *10*, 86.
3. Albelda, S.M. (2024). CAR T cell therapy for patients with solid tumours: key lessons to learn and unlearn. Nat. Rev. Clin. Oncol. *21*, 47–66.
4. Yu, L., Huang, L., Lin, D., Lai, X., Wu, L., Liao, X., Liu, J., Zeng, Y., Liang, L., Zhang, G., et al. (2022). GD2-specific chimeric antigen receptor-modified T cells for the treatment of refractory and/or recurrent neuroblastoma in pediatric patients. J. Cancer Res. Clin. Oncol. *148*, 2643–2652.
5. Nazha, B., Inal, C., and Owonikoko, T.K. (2020). Disialoganglioside GD2 Expression in Solid Tumors and Role as a Target for Cancer Therapy. Front. Oncol. *10*, 1000.
6. Neuroblastoma Survival Rates https://www.cancer.org/cancer/types/neuroblastoma/detection-diagnosis-staging/survival-rates.html.
7. Richards, R.M., Sotillo, E., and Majzner, R.G. (2018). CAR T cell therapy for neuroblastoma. Front. Immunol. *9*, 2380.
8. Kaczanowska, S., Murty, T., Alimadadi, A., Contreras, C.F., Duault, C., Subrahmanyam, P.B., Reynolds, W., Gutierrez, N.A., Baskar, R., Wu, C.J., et al. (2024). Immune determinants of CAR-T cell expansion in solid tumor patients receiving GD2 CAR-T cell therapy. Cancer Cell *42*, 35–51.e8. https://doi.org/10.1016/j.ccell.2023.11.011.
9. Locatelli, F., Pagliara, D., De Ioris, M.A., Becilli, M., Del Baldo, G., Serra, A., Mastronuzzi, A., Cefalo, M.G., Li Pira, G., Leone, G., et al. (2025). GD2-targeting CAR T cells in high-risk neuroblastoma: a phase 1/2 trial. Nat. Med. *31*, 3689–3699.
10. Cao, G., Hu, Y., Pan, T., Tang, E., Asby, N., Althaus, T., Wan, J., Riedell, P.A., Bishop, M.R., Kline, J.P., et al. (2025). Two-stage CD8+ CAR T-cell differentiation in patients with large B-cell lymphoma. Nat. Commun *16*, 4205.
11. Gattinoni, L., Lugli, E., Ji, Y., Pos, Z., Paulos, C.M., Quigley, M.F., Almeida, J.R., Gostick, E., Yu, Z., Carpenito, C., et al. (2011). A human memory T cell subset with stem cell–like properties. Nat. Med. *17*, 1290–1297.
12. Xu, Y., Zhang, M., Ramos, C.A., Durett, A., Liu, E., Dakhova, O., Liu, H., Creighton, C.J., Gee, A.P., Heslop, H.E., et al. (2014). Closely related T-memory stem cells correlate with in vivo expansion of CAR.CD19-T cells and are preserved by IL-7 and IL-15. Blood *123*, 3750–3759.
13. Gnanaprakasam, J.N.R., Kushwaha, B., Liu, L., Chen, X., Kang, S., Wang, T., Cassel, T.A., Adams, C.M., Higashi, R.M., Scott, D.A., et al. (2023). Asparagine restriction enhances CD8+ T cell metabolic fitness and antitumoral functionality through an NRF2-dependent stress response. Nat. Metab. *5*, 1423–1439.
14. Cappabianca, D., Pham, D., Forsberg, M.H., Bugel, M., Tommasi, A., Lauer, A., Vidugiriene, J., Hrdlicka, B., McHale, A., Sodji, Q.H., et al. (2024). Metabolic priming of GD2 TRAC-CAR T cells during manufacturing promotes memory phenotypes while enhancing persistence. Mol. Ther. Methods Clin. Dev. *32*, 101249.
15. Shen, L., Xiao, Y., Zhang, C., Li, S., Teng, X., Cui, L., Liu, T., Wu, N., and Lu, Z. (2022). Metabolic reprogramming by ex vivo glutamine inhibition endows CAR-T cells with less-differentiated phenotype and persistent antitumor activity. Cancer Lett. *538*, 215710.
16. Amini, A., and Veraitch, F. (2019). Glucose deprivation enriches for central memory T cells during chimeric antigen receptor-T cell expansion. Cytotherapy *21*, S30–S31.
17. Dai, Y., Liu, Y., An, L., Zhong, F., Zhang, X., and Lou, S. (2024). Afatinib boosts CAR-T cell antitumor therapeutic efficacy via metabolism and fate reprogramming. J. Immunother. Cancer *12*, e009949.
18. Zhang, X., Zhang, C., Lu, S., Dong, J., Tang, N., Wang, Y., Han, W., Pan, X., Zhang, X., Liu, D., et al. (2024). Miltefosine reinvigorates exhausted T cells by targeting their bioenergetic state. Cell Rep. Med. *5*, 101869. https://doi.org/10.1016/j.xcrm.2024.101869.
19. Pilipow, K., Scamardella, E., Puccio, S., Gautam, S., De Paoli, F., Mazza, E.M., De Simone, G., Polletti, S., Buccilli, M., Zanon, V., et al. (2018). Antioxidant metabolism regulates CD8+ T memory stem cell formation and antitumor immunity. JCI Insight *3*, e122299. https://doi.org/10.1172/jci.insight.122299.
20. Zhu, M., Han, Y., Gu, T., Wang, R., Si, X., Kong, D., Zhao, P., Wang, X., Li, J., Zhai, X., et al. (2024). Class I HDAC inhibitors enhance antitumor efficacy and persistence of CAR-T cells by activation of the Wnt pathway. Cell Rep. *43*, 114065.
21. Gryder, B.E., Sodji, Q.H., and Oyelere, A.K. (2012). Targeted cancer therapy: giving histone deacetylase inhibitors all they need to succeed. Future Med. Chem. *4*, 505–524.
22. Verdin, E., Dequiedt, F., and Kasler, H.G. (2003). Class II histone deacetylases: versatile regulators. Trends Genet. *19*, 286–293.
23. Watanabe, N., and McKenna, M.K. (2022). Generation of CAR T-cells using γ-retroviral vector. Methods Cell Biol. *167*, 171–183.
24. McCarron, A., Donnelley, M., McIntyre, C., and Parsons, D. (2016). Challenges of up-scaling lentivirus production and processing. J. Biotechnol. *240*, 23–30.
25. Schober, K., Müller, T.R., Gökmen, F., Grassmann, S., Effenberger, M., Poltorak, M., Stemberger, C., Schumann, K., Roth, T.L., Marson, A., and Busch, D.H. (2019). Orthotopic replacement of T-cell receptor α- and β-chains with preservation of near-physiological T-cell function. Nat. Biomed. Eng. *3*, 974–984.
26. Mueller, K.P., Piscopo, N.J., Forsberg, M.H., Saraspe, L.A., Das, A., Russell, B., Smerchansky, M., Cappabianca, D., Shi, L., Shankar, K., et al. (2022). Production and characterization of virus-free, CRISPR-CAR T cells capable of inducing solid tumor regression. J. Immunother. Cancer *10*, e004446. https://doi.org/10.1136/jitc-2021-004446.

27. Foy, S.P., Jacoby, K., Bota, D.A., Hunter, T., Pan, Z., Stawiski, E., Ma, Y., Lu, W., Peng, S., Wang, C.L., et al. (2022). Non-viral precision T cell receptor replacement for personalized cell therapy. Nature *615*, 687–696.

28. Gargett, T., Yu, W., Dotti, G., Yvon, E.S., Christo, S.N., Hayball, J.D., Lewis, I.D., Brenner, M.K., and Brown, M.P. (2016). GD2-specific CAR T Cells Undergo Potent Activation and Deletion Following Antigen Encounter but can be Protected From Activation-induced Cell Death by PD-1 Blockade. Mol. Ther. *24*, 1135–1149.

29. Eyquem, J., Mansilla-Soto, J., Giavridis, T., van der Stegen, S.J.C., Hamieh, M., Cunanan, K.M., Odak, A., Gönen, M., and Sadelain, M. (2017). Targeting a CAR to the TRAC locus with CRISPR/Cas9 enhances tumour rejection. Nature *543*, 113–117.

30. Pham, D.L., Cappabianca, D., Forsberg, M.H., Weaver, C., Mueller, K.P., Tommasi, A., Vidugiriene, J., Lauer, A., Sylvester, K., Lika, J., et al. (2025). Label-free metabolic imaging monitors the fitness of chimeric antigen receptor T cells. Nat. Biomed. Eng. 1–18. https://doi.org/10.1038/s41551-025-01504-7.

31. Tommasi, A., Cappabianca, D., Bugel, M., Gimse, K., Lund-Peterson, K., Shrestha, H., Arutyunov, D., Williams, J.A., Police, S.R., Indurthi, V., et al. (2025). Efficient nonviral integration of large transgenes into human T cells using Cas9-CLIPT. Mol. Ther. Methods Clin. Dev. *33*, 101437.

32. Cappabianca, D., Li, J., Zheng, Y., Tran, C., Kasparek, K., Mendez, P., Thu, R., Maures, T., Capitini, C.M., Deans, R., and Saha, K. (2024). Non-viral expression of chimeric antigen receptors with multiplex gene editing in primary T cells. Front. Bioeng. Biotechnol. *12*, 1379900. https://doi.org/10.3389/fbioe.2024.1379900.

33. Pieniawska, M., and Iżykowska, K. (2022). Role of histone deacetylases in T-cell development and function. Int. J. Mol. Sci. *23*, 7828.

34. Zhang, Q., Shu, D.Y., Bryan, R.A., Han, J.Y.S., Gulette, G.A., Lo, K., Kim, L.A., and Miller, J.M.L. (2024). Long-term monitoring of oxygen consumption rates in highly differentiated and polarized retinal pigment epithelial cultures. J. Vis. Exp. *10*, 3791–67038.

35. Minárik, P., Tomaskova, N., Kollárová, M., and Antalik, M. (2002). Malate dehydrogenases-structure and function. Gen. Physiol. Biophys. *21*, 257–266.

36. Passarella, S., de Bari, L., Valenti, D., Pizzuto, R., Paventi, G., and Atlante, A. (2008). Mitochondria and L-lactate metabolism. FEBS Lett. *582*, 3569–3576.

37. Desdín-Micó, G., Soto-Heredero, G., and Mittelbrunn, M. (2018). Mitochondrial activity in T cells. Mitochondrion *41*, 51–57.

38. Lisci, M., and Griffiths, G.M. (2023). Arming a killer: mitochondrial regulation of CD8+ T cell cytotoxicity. Trends Cell Biol. *33*, 138–147.

39. Gattinoni, L., Speiser, D.E., Lichterfeld, M., and Bonini, C. (2017). T memory stem cells in health and disease. Nat. Med. *23*, 18–27.

40. Jiang, D., Mo, Q., Shao, H., Meng, J., Zhong, R., Ji, X., Liang, C., Lin, W., Chen, F., and Dong, M. (2023). Epigenetically silenced DACT3 promotes tumor growth via affecting Wnt/beta-catenin signaling and supports chidamide plus azacitidine therapy in acute myeloid leukemia. Preprint at bioRxiv. https://doi.org/10.1101/2023.01.09.523194.

41. He, B., Wang, Q., Liu, X., Lu, Z., Han, J., Pan, C., Carter, B.Z., Liu, Q., Xu, N., and Zhou, H. (2020). A novel HDAC inhibitor chidamide combined with imatinib synergistically targets tyrosine kinase inhibitor resistant chronic myeloid leukemia cells. Biomed. Pharmacother. *129*, 110390.

42. Zhao, L., Sun, L., Kong, D., Cao, R., Guo, Z., Guo, D., Li, Q., Hao, J., Li, Y., and Emails, L. (2025). Chidamide and venetoclax synergistically regulate the Wnt/β-catenin pathway by MYCN/DKK3 in B-ALL. Ann. Hematol. *104*, 489–501.

43. Hsu, S.C., Galceran, J., and Grosschedl, R. (1998). Modulation of transcriptional regulation by LEF-1 in response to Wnt-1 signaling and association with beta-catenin. Mol. Cell Biol. *18*, 4807–4818.

44. Grumolato, L., Liu, G., Haremaki, T., Mungamuri, S.K., Mong, P., Akiri, G., Lopez-Bergami, P., Arita, A., Anouar, Y., Mlodzik, M., et al. (2013). β-Catenin-independent activation of TCF1/LEF1 in human hematopoietic tumor cells through interaction with ATF2 transcription factors. PLoS Genet. *9*, e1003603.

45. Wozniak, M.B., Villuendas, R., Bischoff, J.R., Aparicio, C.B., Martínez Leal, J.F., de La Cueva, P., Rodriguez, M.E., Herreros, B., Martin-Perez, D., Longo, M.I., et al. (2010). Vorinostat interferes with the signaling transduction pathway of T-cell receptor and synergizes with phosphoinositide-3 kinase inhibitors in cutaneous T-cell lymphoma. Haematologica *95*, 613–621.

46. Voehringer, D., Blaser, C., Brawand, P., Raulet, D.H., Hanke, T., and Pircher, H. (2001). Viral infections induce abundant numbers of senescent CD8 T cells. J. Immunol. *167*, 4838–4843.

47. Voehringer, D., Koschella, M., and Pircher, H. (2002). Lack of proliferative capacity of human effector and memory T cells expressing killer cell lectinlike receptor G1 (KLRG1). Blood *100*, 3698–3702.

48. Schwartzkopff, S., Gründemann, C., Schweier, O., Rosshart, S., Karjalainen, K.E., Becker, K.-F., and Pircher, H. (2007). Tumor-associated E-cadherin mutations affect binding to the killer cell lectin-like receptor G1 in humans. J. Immunol. *179*, 1022–1029.

49. Herndler-Brandstetter, D., Ishigame, H., Shinnakasu, R., Plajer, V., Stecher, C., Zhao, J., Lietzenmayer, M., Kroehling, L., Takumi, A., Kometani, K., et al. (2018). KLRG1+ effector CD8+ T cells lose KLRG1, differentiate into all memory T cell lineages, and convey enhanced protective immunity. Immunity *48*, 716–729.e8.

50. Henson, S.M., Franzese, O., Macaulay, R., Libri, V., Azevedo, R.I., Kiani-Alikhan, S., Plunkett, F.J., Masters, J.E., Jackson, S., Griffiths, S.J., et al. (2009). KLRG1 signaling induces defective Akt (ser473) phosphorylation and proliferative dysfunction of highly differentiated CD8+ T cells. Blood *113*, 6619–6628.

51. Rosshart, S., Hofmann, M., Schweier, O., Pfaff, A.-K., Yoshimoto, K., Takeuchi, T., Molnar, E., Schamel, W.W., and Pircher, H. (2008). Interaction of KLRG1 with E-cadherin: new functional and structural insights. Eur. J. Immunol. *38*, 3354–3364.

52. Lammens, T., Swerts, K., Derycke, L., De Craemer, A., De Brouwer, S., De Preter, K., Van Roy, N., Vandesompele, J., Speleman, F., Philippé, J., et al. (2012). N-cadherin in neuroblastoma disease: expression and clinical significance. PLoS One *7*, e31206.

53. Yi, F., Cohen, T., Zimmerman, N., Dündar, F., Zumbo, P., Eltilib, R., Brophy, E.J., Arkin, H., Feucht, J., Gormally, M.V., et al. (2025). CAR-engineered lymphocyte persistence is governed by a FAS ligand–FAS autoregulatory circuit. Nat. Cancer *6*, 1638–1655.

54. Bai, Z., Woodhouse, S., Zhao, Z., Arya, R., Govek, K., Kim, D., Lundh, S., Baysoy, A., Sun, H., Deng, Y., et al. (2022). Single-cell antigen-specific landscape of CAR T infusion product identifies determinants of CD19-positive relapse in patients with ALL. Sci. Adv. *8*, eabj2820.

55. Liu, W., Mei, T., Jiang, Y., Wang, J., Li, M., Wang, L., Meng, Z., Qin, T., and Huang, D. (2025). Chidamide suppresses macrophage-mediated immune evasion and tumor progression in small cell lung cancer by targeting the STAT4/CCL2 signaling pathway. Cancer Biol. Med. *22*, 1578–1604.

56. Zhao, B., and He, T. (2015). Chidamide, a histone deacetylase inhibitor, functions as a tumor inhibitor by modulating the ratio of Bax/Bcl-2 and P21 in pancreatic cancer. Oncol. Rep. *33*, 304–310.

57. He, M., Qiao, Z., Wang, Y., Kuai, Q., Li, C., Wang, Y., Jiang, X., Wang, X., Li, W., He, M., et al. (2016). Chidamide inhibits aerobic metabolism to induce pancreatic cancer cell growth arrest by promoting Mcl-1 degradation. PLoS One *11*, e0166896.

58. Hurtado, E., Núñez-Álvarez, Y., Muñoz, M., Gutiérrez-Caballero, C., Casas, J., Pendás, A.M., Peinado, M.A., and Suelves, M. (2021). HDAC11 is a novel regulator of fatty acid oxidative metabolism in skeletal muscle. FEBS J. *288*, 902–919.

59. Oehme, I., Linke, J.-P., Böck, B.C., Milde, T., Lodrini, M., Hartenstein, B., Wiegand, I., Eckert, C., Roth, W., Kool, M., et al. (2013). Histone deacetylase 10 promotes autophagy-mediated cell survival. Proc. Natl. Acad. Sci. USA *110*, E2592–E2601.

60. Amitrano, A.M., and Kim, M. (2023). Metabolic challenges in anticancer CD8 T cell functions. Immune Netw. *23*, e9.

61. Simula, L., Fumagalli, M., Vimeux, L., Rajnpreht, I., Icard, P., Birsen, G., An, D., Pendino, F., Rouault, A., Bercovici, N., et al. (2024). Mitochondrial metabolism sustains CD8+ T cell migration for an efficient infiltration into solid tumors. Nat. Commun. *15*, 2203.

62. Franco, F., Bevilacqua, A., Wu, R.-M., Kao, K.-C., Lin, C.-P., Rousseau, L., Peng, F.-T., Chuang, Y.-M., Peng, J.-J., Park, J., et al. (2023). Regulatory circuits of mitophagy restrict distinct modes of cell death during memory CD8+ T cell formation. Sci. Immunol. *8*, eadf7579.

63. Jia, W., Pua, H.H., Li, Q.-J., and He, Y.-W. (2011). Autophagy regulates endoplasmic reticulum homeostasis and calcium mobilization in T lymphocytes. J. Immunol. *186*, 1564–1574.

64. Deshpande, S., Abdollahi, M., Wang, M., Lanting, L., Kato, M., and Natarajan, R. (2018). Reduced autophagy by a microRNA-mediated signaling cascade in diabetes-induced renal glomerular hypertrophy. Sci. Rep. *8*, 6954.

65. Teng, X., Shao, M., Guo, X., Cheng, T., Qian, P., and Huang, H. (2023). Autophagy inhibition prevents CAR-T exhaustion and terminal differentiation via TCF7 accumulation. Blood *142*, 4823.

66. Toulany, M., Dittmann, K., Baumann, M., and Rodemann, H.P. (2005). Radiosensitization of Ras-mutated human tumor cells in vitro by the specific EGF receptor antagonist BIBX1382BS. Radiother. Oncol. *74*, 117–129.